The Astrophysical Journal, 743:145 (8pp), 2011 December 20 doi:10.1088/0004-637X/743/2/145

THE SOLAR DECIMETRIC SPIKE BURST OF 2006 DECEMBER 6: POSSIBLE EVIDENCE FOR FIELD-ALIGNED POTENTIAL DROPS IN POST-ERUPTION LOOPS

E. W. Cliver[1,2], S. M. White[1,3], and K. S. Balasubramaniam[1,3]
[1] Space Vehicles Directorate, Air Force Research Laboratory, Hanscom AFB, MA, USA
[2] Air Force Research Laboratory, Sunspot, NM 88349, USA
[3] Kirtland AFB, Albuquerque, NM 87117, USA
Received 2011 June 9; accepted 2011 August 26; published 2011 December 1

Abstract

A 1.4 GHz solar radio burst associated with a 3B/X6 eruptive flare on 2006 December 6 had the highest peak flux density ($\sim 10^6$ sfu) of any event yet recorded at this frequency. The decimetric event characteristics during the brightest emission phase (numerous intense, short-lived, narrow-band bursts that overlapped to form a continuous spectrum) suggest electron cyclotron maser (ECM) emission. The peak 1.4 GHz emission did not occur during the flare impulsive phase but rather ∼45 minutes later, in association with post-eruption loop activity seen in Hα and by the *Hinode* EUV Imaging Spectrometer. During the Waves/LASCO era, three other delayed bursts with peak intensities $>10^5$ sfu in the 1.0–1.6 GHz (*L*-band) frequency range have been reported that appear to have characteristics similar to the December 6 burst. In each of these three cases, high-frequency type IV bursts were reported in a range from ∼150 to ∼1500 MHz. Assuming a common ECM emission mechanism across this frequency range implies a broad span of source heights in the associated post-eruption loop systems. Difficulties with an ECM interpretation for these events include the generation of the lower frequency component of the type IVs and the long-standing problem of escape of the ECM emission from the loops. Magnetic-field-aligned potential drops, analogous to those observed for Earth's auroral kilometric radiation, could plausibly remove both of these objections to ECM emission.

Key words: solar-terrestrial relations – Sun: coronal mass ejections (CMEs) – Sun: flares – Sun: radio radiation

Online-only material: animations, color figures

1. INTRODUCTION

The great radio burst produced by the 3B/X6 flare on 2006 December 6 demonstrated the ability of solar radio emission to affect directly the use of modern technologies. The 1.4 GHz flux in this event recorded by the Owens Valley Solar Array (OVSA) reached a peak of $\sim 10^6$ sfu (Gary 2008; 1 solar flux unit (sfu) = 1×10^{-22} W m^{-2} Hz^{-1}), strong enough to cause a significant disruption of Global Positioning Service signals (Cerutti et al. 2008; Kinter et al. 2009). Cerutti et al. (2008) noted that this burst was nearly an order of magnitude larger than that of any previously reported event at this frequency. The great decimetric burst was also observed by the Frequency Agile Solar Radio telescope Subsystem Testbed (FST; Liu et al. 2007) at Owens Valley. During the brightest emission in the December 6 event, the FST, which directly samples the 1.0–1.5 GHz frequency range with a Gigabit-per-second digitizer for 100 μs every 20 ms, recorded many hundreds of intense narrowband (3–4 MHz) spike bursts per second in the GPS frequency range, with individual spikes having durations of less than 20 ms (Gary 2008; D. E. Gary et al. 2011, in preparation).

Such "spike" bursts in the decimetric range have been studied since the 1960s (Dröge 1967, 1977; Slottje 1978, 1980, 1981; Benz 1986). They typically have durations of less than 100 ms, high brightness temperatures (up to 10^{15} K), and narrow band-widths ($\lesssim$10 MHz). Individual narrowband bursts can occur in dense clusters that overlap to form a continuous broadband spectrum. Spike bursts offer great promise and great challenge for solar physics—great promise because they are potentially revealing of the time/spatial structure of the particle acceleration process in solar flares (Slottje 1978; Benz 1985; Dąbrowski & Benz 2009; Bárta & Karlický 2001; Karlický & Bárta 2011) and/or the plasma/field characteristics of the acceleration/emitting region (Benz 2004). The extreme burst intensities in spike bursts indicate a coherent emission process, such as plasma emission (Zheleznyakov & Zaitsev 1975; Kuijpers et al. 1981) or electron cyclotron maser (ECM) emission (Wu & Lee 1979; Holman et al. 1980; Melrose & Dulk 1982). The plasma mechanism accounts for solar type III bursts while ECM emission is the favored interpretation of both Jupiter's decametric radio emission and Earth's auroral kilometric radiation (AKR; Melrose 2009). D. E. Gary et al. (2011, in preparation) interpret the spikes in the December 6 event in terms of ECM emission. Plasma emission is based on the "bump-on-tail" instability ($\partial f/\partial v_{||} > 0$) while the free energy in the ECM process is derived from positive $\partial f/\partial v_{\perp}$ (in the usual case of a loss-cone driven maser). As of yet neither the plasma nor the ECM emission mechanism has been fully successful in explaining the characteristics of solar spike bursts (e.g., Benz 1986; Messmer & Benz 2000; Battaglia & Benz 2009). The plasma hypothesis is challenged by the small bandwidths and the high brightness temperatures of decimetric spikes (Benz 1986). The condition for ECM emission to occur (electron cyclotron frequency ($\mathbf{f}_{ce}$) $\gtrsim$ plasma frequency ($\mathbf{f}_{pe}$); Melrose & Dulk 1982; Benz 2004; Treumann 2006) does not apply throughout the low corona (Benz 1986, 2004) and is only likely to be satisfied either in strong-field regions just above sunspot umbrae or in low-density ducts in the low corona.

The ECM emission mechanism has an additional problem at the Sun. It has long been recognized (Holman et al. 1980; Melrose & Dulk 1982) that escape of fundamental ECM emission is difficult, if not impossible, because of thermal gyro-absorption at the second harmonic in the overlying plasma. Various solutions (e.g., emission at harmonics $\geqslant$2 or in the

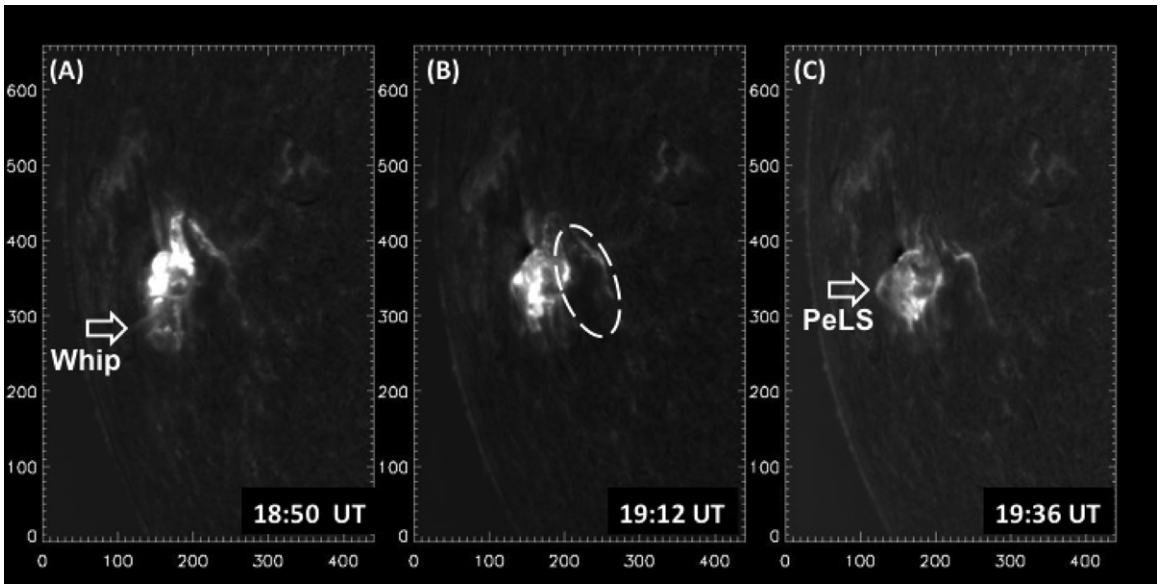

Figure 1. Hα images at 18:50 UT (a), 19:12 UT (b), and 19:36 UT (c) of the 3B/X6 flare on 2006 December 6 taken by the prototype Improved Solar Observing Optical Network (ISOON) telescope (Neidig et al. 1998) at the National Solar Observatory/Sacramento Peak. The arrow in panel (a) points to a ray that exhibited a whip-like movement toward the south at 18:56 UT. The dashed oval in panel (b) indicates the two-ribbon flare linked to the Moreton wave analyzed by Balasubramaniam et al. (2010). The post-eruption loop system (PeLS) associated with the great decimetric burst is indicated in panel (c).

O-mode rather than fundamental emission in the *X*-mode (Melrose et al. 1984); "windows" at parallel or perpendicular propagation where some emission can escape (Holman et al. 1980; Robinson 1989); tunneling through the second harmonic absorption layer and re-emission at >2 $\mathbf{f}_{ce}$ (McKean et al. 1989)) have been proposed for this problem, but none has been generally accepted. Thus, both the nature of spike bursts and the escape of ECM emission at the Sun remain in question.

Accepting, on the basis of the D. E. Gary et al. (2011, in preparation) analysis, that the brightest 1–2 GHz burst components in the 2006 December 6 burst are due to ECM emission, we examine the circumstances under which this intense decimetric burst arose and search for other examples of such events. In particular, we investigate the implications of the requirement that $\mathbf{f}_{ce} \gtrsim \mathbf{f}_{pe}$ for ECM emission to be effective.

Our analysis is presented in Section 2 and the results are interpreted in Section 3 and summarized and discussed in Section 4.

2. ANALYSIS

2.1. 2006 December 6 Event

The 3B/X6 flare in active region (AR) 10930 (Figure 1) has been discussed in detail by Balasubramaniam et al. (2010). Those authors attributed a solar Moreton wave to the eruption of an arcade (indicated by the dashed oval in panel (b)) in the western part of the AR beginning at ~18:40 UT. The main flare, with soft X-ray maximum at 18:47 UT, was located in the strong-field region to the east of this arcade. The two-ribbon flares in the eastern and western portions of 10930 shared a common flare ribbon. The Hα filtergram in panel (a) was taken at 18:50 UT, shortly after flare maximum, and the image in panel (c) was taken at 19:36 UT, near the peak of the most intense 1.4 GHz emission.

Figure 2(a) shows the Sagamore Hill time intensity profile (1 s time resolution) of the radio outburst for the five highest discrete frequencies (1.4 GHz, 2.7 GHz, 5.0 GHz, 8.8 GHz, and 15.4 GHz) monitored by the Radio Solar Telescope Network (RSTN) of the US Air Force. Figure 3 contains a short section of the Owens Valley FST record showing the complex temporal and frequency structure during the time of peak *L*-band (1.0–1.6 GHz) emission (D. E. Gary et al. 2011, in preparation). It is important to note that such emission is not seen continuously from ~19:15 to ~19:40 UT. There are intervals with broader bandwidth emission and/or reduced intensities.

The spectral maximum in the centimeter wavelength range for this event alternates between 5.0 and 8.8 GHz on the initial rise of the event from ~18:30 to 18:43 UT, and then drifts downward from 15.4 GHz (during ~18:43–18:48 UT) to 8.8 GHz (during ~18:48–19:13 UT) to 5.0 GHz (after ~19:13 UT). Decimetric spike activity in the FST record is most prominent after ~19:16 UT when the great burst that reached a peak flux density of $\sim 10^6$ sfu (as measured by the OVSA) began. The Sagamore Hill 1.4 GHz intensity is intermittently saturated at a level of $\sim 1.4 \times 10^5$ sfu after ~19:16 UT, particularly from ~19:30 to 19:40 UT (Figure 2(a)). We note that the most intense *L*-band emission occurred ~45 minutes after the flare impulsive phase, which is generally taken to be the most energetic phase of a flare (e.g., Hudson 2011).

The principal activity in Hα images of the 3B/X6 flare during the interval of strong 1.4 GHz emission (~18:50–19:40 UT) involved the post-eruption loop system (PeLS) in the eastern part of AR 10930 (Figure 1(c)). At 18:56 UT, a whip-like movement toward the south of a ray emanating from 10930 (indicated by the arrow in Figure 1(a)) raises the possibility of a secondary eruption in this event (after the primary eruption at ~18:40 UT). Beginning around 18:50 UT, we see the apparent rise of a bright feature on the east edge of the flare that evolves to form the central part of the PeLS indicated in Figure 1(c). From ~19:15 UT to ~19:40 UT, the evolution of the loop system is accompanied by the most intense part of the complex 1.4 GHz burst (see Movie M1 in the Electronic Supplement (ES). It seems clear that the two phenomena—intense decimetric activity and post-eruption loop (Švestka 2007) formation—are related. The Hα images of the post-eruption loops are substantiated by an early *Hinode* EUV Imaging Spectrometer (EIS; Culhane

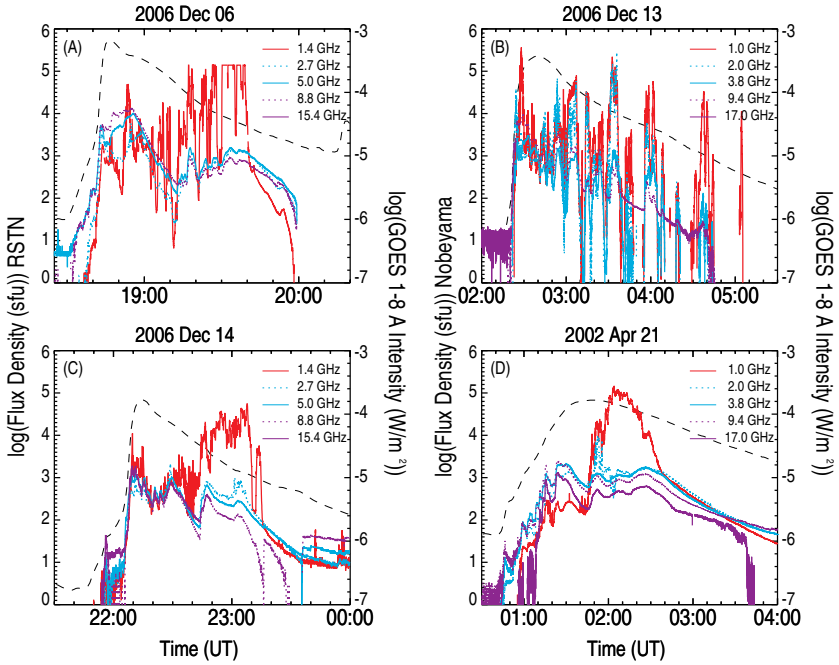

Figure 2. Great ($>10^5$ sfu) decimetric radio bursts on (a) 2006 December 6; (b) 2006 December 13; (c) 2006 December 14; and (d) 2002 April 21. The data are plotted at 1 s time resolution. For the event on December 14, OVSA recorded a burst at 1.6 GHz (not shown) with a peak intensity of $\sim 1.5 \times 10^5$ sfu at 1.6 GHz. The dashed gray line in each of the panels is the time-intensity profile of the associated *GOES* 1–8 Å burst.

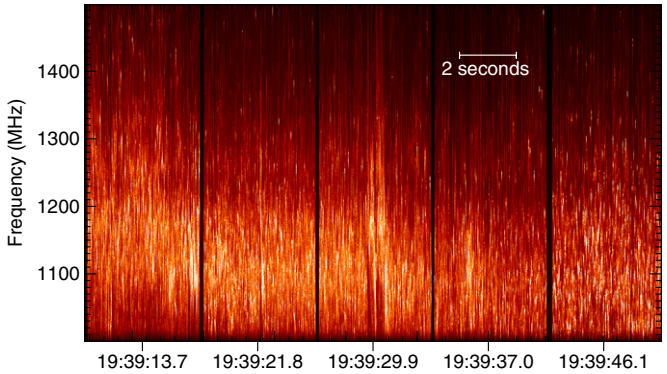

Figure 3. Four-second scans in right circular polarization, with 4 s gaps between them (not shown). The time resolution is 20 ms and the frequency resolution is 1 MHz. Time labels on the bottom axis are for the center of each 4 s scan.

et al. 2007) scan of 195 Å intensity and Doppler velocity from 19:15–23:44 UT that shows such loops over both the eastern and western arcades (see Figure 16 in Balasubramaniam et al. 2010). The *Hinode* Soft X-ray Telescope (Tsuneta et al. 2008) Ca II/H record (Movie M2 in the ES; 13:15–23:58 UT) shows that the post-eruption arcade is well developed at the onset of the most intense *L*-band emission.

While coronal images from the Large Angle Spectroscopic Coronagraph (LASCO; Brueckner et al. 1995) on the *Solar and Heliospheric Observatory* (*SOHO*) are not available for the time of the 3B/X6 flare, there is ample evidence (Balasubramaniam et al. 2010) that this event was associated with a coronal mass ejection (CME). The evidence includes the observation of (1) CME remnants above the southeast limb at 20:12 UT, at the end of a LASCO data gap (http://cdaw.gsfc.nasa.gov/CME_list/); (2) an interplanetary (IP) type II radio burst (http://lep694.gsfc.nasa.gov/waves/waves.html; Bougeret et al. 1995); and (3) a >100 MeV SEP event observed by the *GOES* satellite late on December 6.

2.2. Additional Intense and Delayed L-band Bursts

Cerutti et al. (2008) and Gary (2008) noted that two other flares from region 10930, on December 13 and 14, were associated with great ($>10^5$ sfu) decimetric radio bursts. On December 13, the Nobeyama polarimeter at 1 GHz recorded a burst of 4.4×10^5 sfu (1 s data; Figure 2(b)). In this case, a great decimetric burst peaked at 02:28 UT near the impulsive phase peak of the 4B/X3 flare as determined by the higher fixed frequencies. Approximately 1 hr later, however, a complex 1 GHz burst with a peak intensity of $\sim 2.8 \times 10^5$ sfu was observed. On December 14, OVSA, including the FST, recorded an intense burst beginning at ~22:50 UT, ~35 minutes after the 2B (X1) Hα maximum, with a peak intensity of $\sim 1.5 \times 10^5$ sfu at 1.6 GHz (Gary 2008). The corresponding RSTN data from Learmonth (Figure 2(c)) show a peak of only $\sim 6 \times 10^4$ sfu at 1.4 GHz. The FST record of this intense delayed burst reveals a range of behavior, but, in particular, during the time of peak emission (near 1.6 GHz at 23:05 UT), spikes are the brightest feature present. For completeness, we searched both the 1 GHz burst archive of the Nobeyama Solar Radio Observatory (http://solar.nro.nao.ac.jp/) and the RSTN 1415 MHz database during the Waves/LASCO era (1996–present) for any other bursts in the 1.0–1.6 GHz frequency range with peak flux densities $\geqslant 10^5$ sfu and significant ($\gtrsim$30 minute) delays from the flare impulsive phase. We uncovered one such event, a 1 GHz burst with peak intensity of $\sim 1.5 \times 10^5$ sfu that was associated with a 1F/X1 flare on 2002 April 21 (Figure 2(d)).

Each of these events was associated with a high speed CME (21 April (2393 km s^{-1}), December 13 (1774 km s^{-1}), December 14 (1042 km s^{-1})), an IP type II burst, and a >100 MeV SEP event. The presence of a CME and the available spacecraft evidence from the *SOHO* Extreme-ultraviolet Imaging Telescope (Delaboudinière et al. 1995), the *Reuven Ramaty High Energy Solar Spectroscopic Imager* (*RHESSI*; Lin et al. 2002), *Hinode* EIS, and *Transition Region and Coronal Explorer*

Table 1
Large Delayed *L*-band (1–1.6 GHz) Bursts, 1996–Present[a]

Date	Imp.[b] Phase (UT)	Hα Location	Hα/X-ray Class	$D_{cim.}$[c] Frequency (MHz)	$D_{cim.}$ Peak Int. (sfu)	$D_{cim.}$[d] Delay (minutes)	CME Speed (km s^{-1})
2002 Apr 21	0115	S14W84	1F/X1	1000(N)	1.50×10^5	35	2393
2006 Dec 6	1845	S06E63	3B/X6	1400(F)	$\sim 10^6$	30	N/A
2006 Dec 13	0230	S06W24	4B/X3	1000(N)	$\sim 2.80 \times 10^5$	20	1774
2006 Dec 14	2210	S06W46	2B/X1	1600(F)	1.50×10^5	35	1042

Notes.
[a] Intense delayed decimetric bursts similar to that on 2006 December 6 were reported by Sagamore Hill at 1.4 GHz on 1973 April 29 (1.65×10^5 sfu, ∼75 minute delay; SGD No. 350, Pt II, p. 63), Kiel at 1 GHz on 1974 July 4 (8.0×10^5 sfu, ∼30 minute delay; SGD No. 360, Pt. I, p. 30 and SGD No. 365, Pt. II, p. 42), and Nobeyama at 1.0 GHz on 1990 April 15 (7.19×10^5 sfu, ∼100 minute delay, http://solar.nro.nao.ac.jp/ and SGD No. 554, Pt II, p. 42). Intense short-duration *L*-band events, occurring during or relatively near the flare impulsive phase were reported on 1992 November 2 (Nobeyama, 1 GHz, 1.04×10^5 sfu; X9.0 maximum at 03:08 UT); 1993 February 8 (Nobeyama, 1 GHz, 5.72×10^5 sfu; C9.2 at 02:42 UT); and 2005 July 11 (San Vito, 1.4 GHz, 1.2×10^5 sfu; C1.0 at 16:37 UT). The 1993 February 8 event appears to be an instrumental artifact and the short duration (∼10 s) of very intense emission in the 1992 November 2 event raises questions about its origins. The 2005 July 11 burst appears to be solar and saturated the San Vito 1.4 GHz flux for about 30 s but the peak flux density was not confirmed by the RSTN stations at Sagamore Hill and Palehua both of which reported peak intensities $\sim 2 \times 10^3$ sfu. Thus, the only certain burst of this type ($\geqslant 10^5$ sfu, flare impulsive phase, *L* band) that we are aware of is that on 2006 December 13 (Nobeyama, 1 GHz, 4.40×10^5 sfu).
[b] Approximate time of the first significant ($>10^3$ sfu) microwave peak.
[c] N = Nobeyama; F = FST (OVSA).
[d] Approximate delay from the first significant microwave peak to the onset of delayed intense ($>10^5$ sfu) *L*-band emission.

(Handy et al. 1999) indicate that in each of these three cases, the delayed decimetric bursts occurred during the post-eruption arcade phase of the X-class flares (December 13: Imada et al. 2007; Attrill et al. 2010; December 14: Harra et al. 2007; McIntosh 2009; 21 April: Gallagher et al. 2002; McKenzie & Savage 2009).

The data for the events on 2006 December 6, 13 (delayed component), and 14 and 2002 April 21 are summarized in Table 1. Although the extreme peak flux densities at *L* band in all of these events indicate a coherent emission process, we know for certain that only the events on December 6 and 14, both recorded by the FST at high temporal and spectral resolution, contained spike bursts. In addition, while the similar delays in the four bursts—and apparent origin in post-eruption loop systems—suggest a common emission mechanism, this need not be the case. In fact, Kundu et al. (2004) attributed the 2002 April 21 event to plasma emission based on its high-intensity, 100% left circular polarization, and broadband (from ∼500 to 2000 MHz) nature. The sense of polarization is relevant because simultaneous 17 GHz nonthermal emission, assumed to be optically thin gyrosynchrotron emission and therefore *X*-mode, had the opposite polarization, suggesting that the 1 GHz emission is *O*-mode as expected for fundamental plasma emission. This polarization evidence is not compelling, however, because it assumes that the 17 GHz and 1 GHz emission in this event originated from regions with the same orientation of the magnetic field to the line of sight, and ignores the possibility of mode coupling altering the observed polarization. Further, as was the case for the December 6 event (Cerutti et al. 2008), large numbers of overlapping spike bursts can mimic broadband emission in radio telescopes with low temporal/spectral resolution.

3. INTERPRETATION

3.1. Electron Trapping in Post-eruption Loops

In Figures 2(a)–(d), the delayed intense *L*-band bursts occur on the rise of weaker "secondary" microwave bursts (Tanaka & Kakinuma 1962). Such delayed microwave peaks, as well as accompanying gradual hard X-ray bursts, have been attributed to particle acceleration at the X-type neutral point in eruptive flares and electron trapping on the most recently formed and least densely populated post-eruption loops (Cliver 1983; Cliver et al. 1986). The soft–hard–harder (SHH) evolution of the hard X-ray spectrum (Kiplinger 1995; Krucker et al. 2008) observed by *RHESSI* for at least one of the delayed decimetric bursts (2002 April 21; Grayson et al. 2009) provides evidence of such trapping (Figure 4(a)). Grayson et al. (2009) also noted spectral hardening during the impulsive phase of the 2006 December 14 event; a data gap occurred from 22:25 to 23:10 UT during the time of the peak *L*-band emission. Similar gaps compromised the *RHESSI* observations of the events on December 6 (Figure 4(b)) and December 13, but in both cases there is evidence of SHH spectral evolution either before or across the data gaps. Thus we suggest that, in certain cases, electrons trapped in post-eruption loops can also give rise to intense decimetric emission via the ECM emission mechanism. Note that, in contrast to the decimetric bursts, the delayed $\geqslant$5 GHz microwave bursts in the events in Figure 2 have relatively smooth profiles and peak intensities of $\lesssim 10^3$ sfu, consistent with gyro-synchrotron emission from trapped electrons. Also, note in Figure 2, particularly in panels (a), (c), and (d), that the intense *L*-band emission appears to ride on top of the microwave bursts, returning to comparable levels after the decimetric outbursts and, in the case of the December 6 event, intermittently during the outburst.

3.2. Condition for Electron Cyclotron Maser Emission: Field-aligned Potential Drop?

Can the $\mathbf{f}_{ce} \gtrsim \mathbf{f}_{pe}$ condition for ECM emission be satisfied for a post-eruption loop source for the intense decimetric events under consideration? Broadband radio observations of these events suggest that the spike emission may be occurring over a relatively wide range of frequencies. We note that Kundu et al. (2004) surmised that a single emission mechanism (plasma emission according to their suggestion) applied for the "high-frequency (HF) type IV" that extended from 130 MHz to ∼2 GHz on 2002 April 21, encompassing the great decimetric

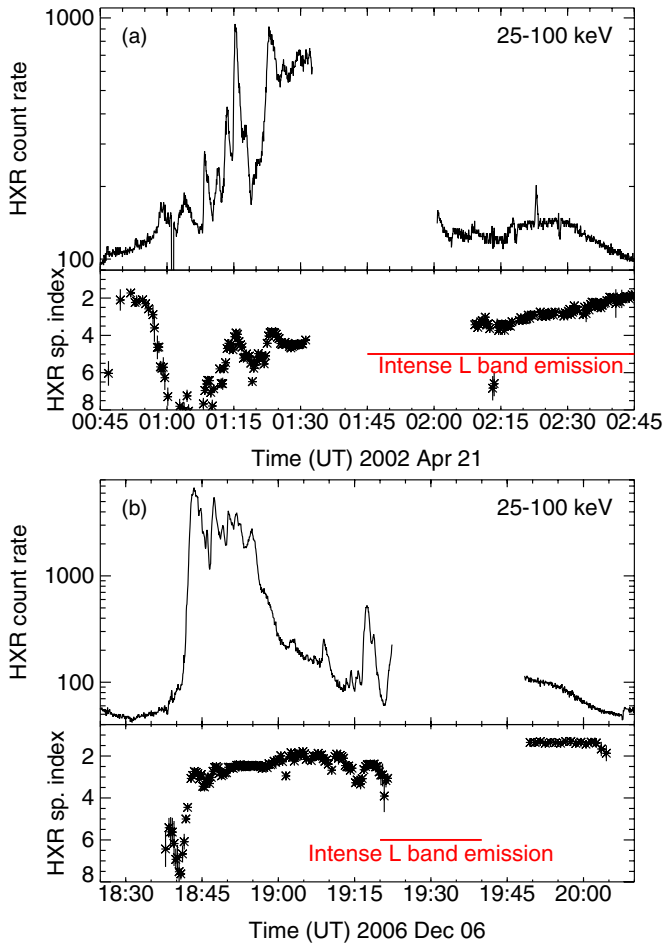

Figure 4. *RHESSI* observations showing evolution of hard X-ray spectra during the times of intense decimetric emission (spanned by the red lines) on (a) 2002 April 21 (see Grayson et al. 2009) and (b) 2006 December 6.

(A color version of this figure is available in the online journal.)

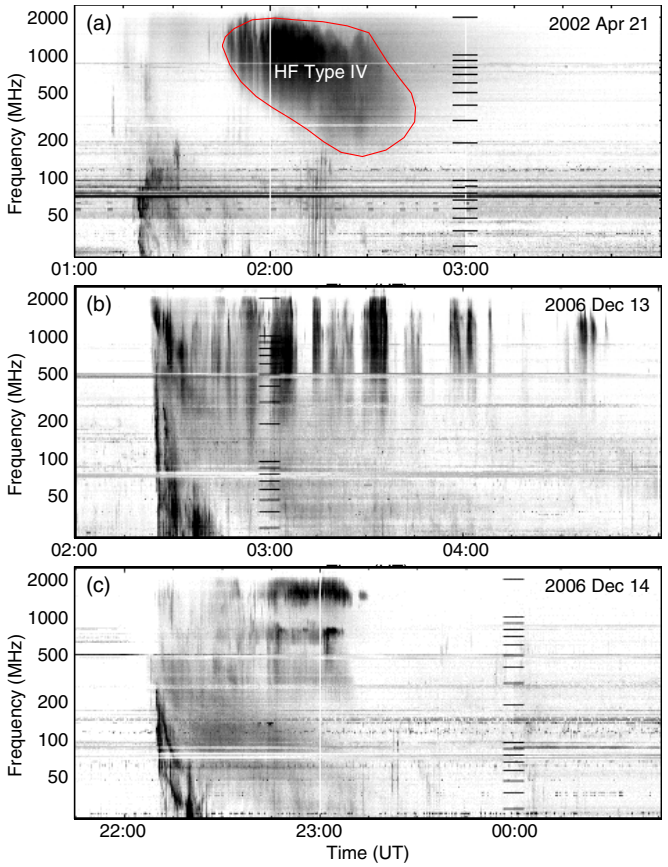

Figure 5. Broadband spectrograms from *Hiraiso* for the high-frequency type IV bursts on (a) 2002 April 21, (b) 2006 December 13, and (c) 2006 December 14. The red line in panel (a) outlines the presumed ECM emission.

(A color version of this figure is available in the online journal.)

burst on that date (Figure 2(d)). The well-defined nature of the HF type IV in the *Hiraiso* spectrogram (Figure 5(a)) suggests a spatially circumscribed source and calls to mind the confinement of the ECM emission source in Earth's auroral plasma cavity (Calvert 1981). Similar HF type IVs were observed for the 2006 December 13 (~150 MHz–1.3 GHz; Figure 5(b)) and December 14 events (~180 MHz–1.6 GHz; Figure 5(c)). For both of these events, as for that on 2002 April 21, Culgoora reported storm radiation (either type I or type III) at lower frequencies during the time of the intense decimetric emission. There are differences between the three events, however. In the December 13 event, the intense broadband emission is intermittent while in the December 14 event, there is a gap in frequency. At first glance, this gap suggests harmonic structure, but for at least some times during the intense *L*-band burst, specifically at ~22:45 UT and ~23:05 UT, the *Hiraiso* record argues against this interpretation.

What field strengths and densities correspond to ECM emission in the frequency range from 130 MHz to 2 GHz? The expression for the electron-cyclotron frequency

$$\mathbf{f}_{ce} = eB/2\pi m_e \quad (1)$$

reduces to

$$\mathbf{f}_{ce}(\mathrm{MHz}) = 2.8\ B(\mathrm{G}). \quad (2)$$

Assuming fundamental emission, the frequency range 130–2000 MHz implies a range in B from ~50 G to ~700 G. Such magnetic field strengths suggest an ECM emission source region ranging over a range of heights in the post-flare loop systems following the four large flares under consideration. During the time of the intense decimetric emission in the 2002 April 21 event (~01:45–02:30 UT), the centroid of coronal hard X-ray emission observed by *RHESSI* moved from a height of $\sim 3.5 \times 10^4$ km to $\sim 6.5 \times 10^4$ km (Gallagher et al. 2002). Using the model of Dulk & Mclean (1978), such heights imply field strengths of ~45 G and ~18 G, respectively, which are consistent, given the uncertainties involved, with the lower end (~50 G) of the inferred range of magnetic field strengths for the late decimetric outbursts.

For ECM emission to occur at any height in the solar atmosphere, the following condition

$$\mathbf{f}_{ce} \gtrsim \mathbf{f}_{pe} \quad (3)$$

must be met (where $\mathbf{f}_{pe}$ (MHz) $= e/2\pi(n_e/m_e\varepsilon_0)^{1/2} = 9 \times 10^{-3}(n(\mathrm{cm}^{-3}))^{\frac{1}{2}}$) (Melrose & Dulk 1982; Benz 2004; Treumann 2006). Thus near the low end of the magnetic field range where $B \sim 50$ G ($\Omega_{ce} = 130$ MHz), we require

$$n < 2 \times 10^8\ \mathrm{cm}^{-3}, \quad (4)$$

while at the stronger field range $B \sim 700$ G ($\mathbf{f}_{ce} = 2000$ MHz) we require

$$n < 5 \times 10^{10}\ \mathrm{cm}^{-3}. \quad (5)$$

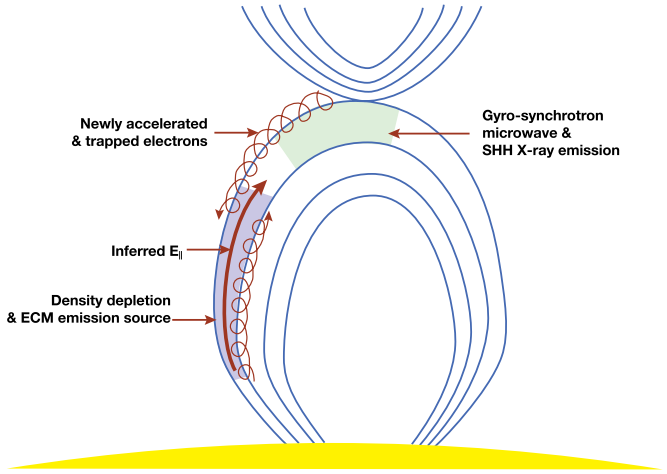

Figure 6. Schematic showing how ring-shell ECM emission might arise in post-eruption loops as a result of strong late-phase reconnection (particle acceleration) at an X-type neutral point (or in a neutral current sheet) and a magnetic field-aligned potential drop (density depletion).

A density of $\lesssim 5 \times 10^{10}$ cm^{-3} would be considered plausible for the hot plasma in a bright post-flare loop system such as was present in the events considered here, although higher densities are often inferred (10^{11} cm^{-3}; e.g., Doschek et al. 1995; Aschwanden & Alexander 2001; Kamio et al. 2003). However, densities $\lesssim 2 \times 10^{8}$ cm^{-3} would be regarded as low for such an environment, so it is more difficult to see how an ECM could operate at frequencies as low as ∼130 MHz in a PeLS. For example, Krucker et al. (2010) deduced a density of $\sim 2 \times 10^{9}$ cm^{-3} for the loop top acceleration region in the partially occulted flare observed by *RHESSI* on 2007 December 31.

Current understanding of Earth's AKR suggests a way in which ECM emission could originate in post-eruption loops at the Sun. In the Earth's magnetosphere, the AKR emission source corresponds to a low-density plasma cavity (Calvert 1981; Hilgers 1992). The density in the cavity can be a factor of ∼30 lower than that of the ambient plasma in the auroral zone (Calvert 1981; Temerin 1984; Persoon et al. 1983; Ergun et al. 2000). Such density depletions are caused by electric fields aligned with Earth's magnetic field (Temerin et al. 1982; Mozer & Kletzing 1998; Ergun et al. 2001). These parallel electric fields accelerate ions outward and electrons earthward to create a local cavity. Assuming that such field-aligned potential drops occur at the Sun and cause similar localized density depletions, a nominal loop top density of $\sim 3 \times 10^{9}$ cm^{-3} is reduced to $\sim 10^{8}$ cm^{-3}, permitting effective operation of the maser instability with $\mathbf{f}_{pe} < \mathbf{f}_{ce}$ for frequencies as low as ∼100 MHz. A factor of 30 density depletion at higher densities implies that ECM emission at frequencies as high as 2000 MHz could occur in source regions with pre-depletion densities $\lesssim 10^{12}$ cm^{-3}.

Our view of the late-phase events with intense *L*-band emission is given in the schematic of Figure 6. The schematic is based on the standard CSHKP (Hudson & Cliver 2001) model of eruptive solar flares (e.g., Forbes 2000). In this picture, gyro-synchrotron and ECM emission can arise simultaneously, consistent with the time profiles in Figure 2 which suggest that the ECM emission is superimposed on a gyro-synchrotron baseline.

4. CONCLUSION

We examined the solar circumstances for the extreme ($\sim 10^{6}$ sfu) decimetric radio burst of 2006 December 6 that occurred during the decay phase of a 3B/X6 flare and three other similarly delayed *L*-band (1.0–1.6 GHz) bursts with peak flux densities $>10^{5}$ sfu that occurred during the Waves/LASCO era, i.e., since 1996. The delays from the impulsive phase in the four events ranged from 20 to 35 minutes. In the 2006 December 6 event, the intense decimetric emission occurred during evolution of the post-eruption arcade as observed in Hα (Figure 1(c); Movie M1 in the ES) and in Ca II (Movie M2).

Particle acceleration in these events appears to occur via magnetic reconnection in the post-eruption phase, in accordance with the standard CSHKP model of eruptive flares. The most plausible acceleration mechanism is a reconnection-driven stochastic process (e.g., Ramaty 1979; Liu et al. 2008) based on magnetic turbulence. Accelerated electrons trapped on the post-eruption loops then give rise to delayed decimetric/microwave bursts (Tanaka & Kakinuma 1962; Cliver 1983) through the gyro-synchrotron emission mechanism and associated gradual hard X-ray bursts (Frost & Dennis 1971; Cliver et al. 1986) via the bremmstrahlung process. In the present study, we have argued, following D. E. Gary et al. (2011, in preparation), that the trapped electrons can also simultaneously give rise to intense decimetric spike bursts via the ECM emission mechanism (Figure 6).

As noted in the introduction, decimetric spike bursts offer insight into the flare acceleration process (Slottje 1978; Benz 1985; Dąbrowski & Benz 2009) and/or the flare environment (Benz 2004). The evidence for electron trapping in these events (SHH X-ray spectral evolution and relatively smooth microwave burst profiles) suggests that the rapid time variation at decimetric wavelengths is not a direct reflection of the flare particle-acceleration process. Rather, the exotic appearance of decimetric spike bursts (Figure 3) is interpreted in terms of the complexity of the emission source region, specifically a proliferation of small amplitude "electron holes" (or "elementary radiation sources") in velocity phase space (Treumann 2006). For an alternative view in which decimetric spike bursts are more intimately related to the acceleration process, see the recent modeling studies of Karlický & Bárta (2011) and Bárta et al. (2011) in which spike bursts are produced via the plasma emission mechanism by electrons accelerated in fragmented current sheets generated by merging plasmoids.

The apparent broad frequency range (∼150–1500 MHz) of the spike emission in the intense delayed HF type IV events we examined, coupled with the $\mathbf{f}_{ce} \gtrsim \mathbf{f}_{pe}$ requirement for ECM emission, lead us to infer density depletions in the coronal loop source regions. We suggest that the same phenomenon occurs at the Sun to produce these depletions as that observed to occur in Earth's magnetosphere in association with AKR—specifically, magnetic-field-aligned potential drops. Fletcher & Hudson (2008) have recently argued that large-scale Alfvén wave pulses generated via reconnection in solar flares could give rise to such field-aligned electric fields in the legs of coronal loops.

Following Melrose & Dulk (1982), early work on applying the ECM emission mechanism to solar radio bursts focused on the loss-cone maser (Wu & Lee 1979). Subsequently, simulations (Pritchett 1984; Pritchett & Strangeway 1985; Winglee & Pritchett 1986; Pritchett et al. 1999) and in situ observations of Earth's magnetosphere (Louarn et al. 1990; Roux et al. 1993; Ergun et al. 1998; Delory et al. 1998; Strangeway et al. 1998)

established the current picture in which "shell" or "horseshoe" electron distributions in velocity phase space are the source of the ECM instability and Earth's AKR. Ergun et al. (2000), Kellett et al. (2002), and Treumann (2006) have suggested that this type of maser should be considered for stellar emissions, including spike bursts from the Sun. In Earth's magnetosphere, the shell distribution is produced by an electric field (of as yet uncertain origin; e.g., Stasiewicz et al. 2000) that is parallel to the ambient magnetic field. As electrons are accelerated downward by the electric field and/or injected downward by the reconnection-driven acceleration process (White et al. 1983, 1986), their pitch angle increases due to the conservation of the first adiabatic invariant and a "ring-shell" or "horseshoe" distribution which is unstable to ECM emission is formed. At the same time the field-aligned potential drop naturally creates a low-density cavity that allows the $\mathbf{f}_{ce} \gtrsim \mathbf{f}_{pe}$ condition to be satisfied.

A long-standing difficulty with ECM emission at the Sun (Holman et al. 1980; Melrose & Dulk 1982; Melrose 1994) is thermal gyro-absorption at the second harmonic by the overlying plasma. As recently as 2009, Melrose concluded a review as follows: "...suggested stellar [solar] applications of ECME will remain questionable until the escape of the radiation is explained convincingly." Ergun et al. (2000) suggest that in stellar atmospheres the density cavity associated with parallel electric fields and ring-shell masers can work as a wave guide or duct to reflect the ECM radiation upward along the loops toward weaker magnetic fields, permitting escape. In the case of AKR, it is believed that the maser radiation is amplified in channels of constant latitude at low altitudes and then refracts upward, still in low-density channels, toward decreasing magnetic field regions where it can escape (e.g., Pritchett et al. 2002; Mutel et al. 2008). The issues involved in the escape of solar spike bursts are discussed in detail by Melrose (1994), and they remain valid here. Refraction in field-aligned ducts will have the effect of channeling the radiation in the magnetic field direction, which minimizes absorption in higher-harmonic layers. We expect that the low-density ducts in the solar corona will be field-aligned as they are in the terrestrial magnetosphere, and that radiation escape is most likely at the higher-altitude end of the duct where density and magnetic field will be lower than in the maser source. The opacity of the second harmonic layer is proportional to the ambient electron density and to the magnetic gradient scale length in the direction of wave propagation. Since both of these quantities are substantially smaller in the case of AKR than they are for the solar corona at 1000 MHz, it seems likely that the radiation will need to be propagating close to the magnetic field direction in the solar case if it is to pass through the second-harmonic layer.

It is puzzling that the great/delayed decimetric bursts are so rare—with only four $>10^5$ sfu *L*-band bursts recorded from 1996 to present—given that the picture we propose (Figure 6) is the standard model for the late phase of large flares. Many other major soft X-ray flares that were not accompanied by such great decimetric bursts (e.g., the October 28 (X18) and 29 (X10) "Halloween" flares of 2003; Gopalswamy et al. 2005) occurred during this interval. The fact that three of the four such bursts during the last 15 years originated in AR 10930 in 2006 December suggests that some peculiarity of ARs or their environs fosters strong late-phase reconnection and particle acceleration and/or field-aligned potential drops (plasma cavities). The nature (e.g., single or multiple/filamentary) and location of such cavities in post-eruption loops, and their spatial relationship to the sources of the concomitant coronal hard X-ray and gyro-synchrotron microwave bursts is only guessed at in Figure 6. Clearly, more and better observations of great spike burst events—by next generation radio telescopes such as the Frequency Agile Solar Radio telescope (Bastian 2004) with high temporal/spatial/spectral resolution—are needed to fully realize the promise of these events as a probe of solar dynamics/conditions.

We acknowledge support from the Air Force Office of Scientific Research through AFRL Task 2301RDA1.

REFERENCES

Aschwanden, M. J., & Alexander, D. 2001, Sol. Phys., 204, 93
Attrill, G. D. R., Harra, L. K., van Driel-Gesztelyi, L., & Wills-Davey, M. J. 2010, Sol. Phys., 264, 119
Balasubramaniam, K. S., Cliver, E.W., Pevtsov, A., et al. 2010, ApJ, 723, 587
Bárta, M., Büchner, K. M., Karlický, M., & Skála, J. 2011, ApJ, 737, 24
Bárta, M., & Karlický, M. 2001, A&A, 379, 1045
Bastian, T. 2004, in Solar & Space Weather Radiophysics, ed. D.E. Gary & C.U. Keller (Dordrecht: Kluwer), 47
Battaglia, M., & Benz, A. O. 2009, A&A, 499, L33
Benz, A. O. 1985, Sol. Phys., 96, 357
Benz, A. O. 1986, Sol. Phys., 104, 99
Benz, A. O. 2004, in Solar & Space Weather Radiophysics, ed. D. E. Gary & C. U. Keller (Dordrecht: Kluwer), 203
Bougeret, J.-L., Kaiser, M. L., Kellogg, P. J., et al. 1995, Space Sci. Rev., 71, 231
Brueckner, G. E., Howard, R. A., Koomen, M. J., et al. 1995, Sol. Phys., 162, 357
Calvert, W. 1981, Geophys. Res. Lett., 8, 919
Cerutti, A. P., Kinter, P. M., Jr., Gary, D. E., et al. 2008, Space Weather, 6, S10D07
Cliver, E. W. 1983, Sol. Phys., 84, 347
Cliver, E. W., Dennis, B. R., Kiplinger, A. L., et al. 1986, ApJ, 305, 920
Culhane, J. L., Harra, L. K., James, A. M., et al. 2007, Sol. Phys., 243, 19
Dąbrowski, B. P., & Benz, A. O. 2009, A&A, 504, 565
Delaboudinière, J. P., Artzner, G. E., Brunaud, J., et al. 1995, Sol. Phys., 162, 291
Delory, G. T., Ergun, R. E., Carlson, C. W., et al. 1998, Geophys. Res. Lett., 25, 2069
Doschek, G. A., Strong, K. T., & Tsuneta, S. 1995, ApJ, 440, 370
Dröge, F. 1967, Z. Astrophys., 66, 214
Dröge, F. 1977, A&A, 57, 285
Dulk, G. A., & McLean, D. J. 1978, Sol. Phys., 57, 279
Ergun, R. E., Carlson, C. W., McFadden, J. P., et al. 1998, Geophys. Res. Lett., 25, 2025
Ergun, R. E., Carlson, C.W., McFadden, J. P., et al. 2000, ApJ, 538, 456
Ergun, R. E., Su, Y.-J., Andersson, L., et al. 2001, Phys. Rev. Lett., 87, 045003
Fletcher, L., & Hudson, H. S. 2008, ApJ, 675, 1645
Forbes, T. 2000, J. Geophys. Res., 105, 23153
Frost, K. J., & Dennis, B. R. 1971, ApJ, 165, 655
Gallagher, P. T., Dennis, B. R., Krucker, S., Schwartz, R. A., & Tolbert, A. K. 2002, Sol. Phys., 210, 341
Gary, D. E. 2008, in Ionospheric Effects Symposium (Proceedings) (JMG Associates Ltd: Sheridan Books), accession No. PB2008-112709
Gopalswamy, N., Barbieri, L., Cliver, E. W., et al. 2005, J. Geophys. Res., 110, A09S00
Grayson, J. A., Krucker, S., & Lin, R. P. 2009, ApJ, 707, 1588
Handy, B. N., Acton, L. W., Kankelborg, C. C., et al. 1999, Sol. Phys., 187, 229
Harra, L. K., Hara, H., Imada, S., et al. 2007, PASJ, 59, S801
Hilgers, A. 1992, Geophys. Res. Lett., 19, 237
Holman, G. D., Eichler, D., & Kundu, M. R. 1980, in IAU Symp. 86, Radio Physics of the Sun, ed. M. R. Kundu & T. E. Gergely (Dordrecht: Reidel), 457
Hudson, H. S. 2011, Space Sci. Rev., 158, 5
Hudson, H. S., & Cliver, E. W. 2001, J. Geophys. Res., 106, 25199
Imada, S., Hara, H., Watanabe, T., et al. 2007, PASJ, 59, S793
Kamio, S., Kurokawa, H., & Ishii, T. T. 2003, Sol. Phys., 215, 127
Karlický, M., & Bárta, M. 2011, ApJ, 733, 107
Kellett, B. J., Bingham, R., Cairns, R. A., & Tsikoudi, V. 2002, MNRAS, 329, 102

Kinter, P. M., Jr., O'Hanlon, B., Gary, D. E., & Kinter, P. M. S. 2009, Radio Sci., 44, RS0A08
Kiplinger, A. L. 1995, ApJ, 453, 973
Krucker, S., Battaglia, M., Cargill, P. J., et al. 2008, A&AR, 16, 155
Krucker, S., Hudson, H. S., Glesener, L., et al. 2010, ApJ, 714, 1108
Kuijpers, J., van der Post, P., & Slottje, C. 1981, A&A, 103, 331
Kundu, M. R., Garimov, V. I., White, S. M., & Krucker, S. 2004, ApJ, 600, 1052
Lin, R. P., Dennis, B. R., Hurford, G. J., et al. 2002, Sol. Phys., 210, 3
Liu, Z., Gary, D. E., Nita, G. M., White, S. M., & Hurford, G. J. 2007, PASP, 119, 303
Liu, W., Petrosian, V., Dennis, B. R., & Jiang, Y. W. 2008, ApJ, 676, 704
Louarn, P., Roux, A., de Féraudy, H., Le Quéau, D., André, M., & Matson, L. 1990, J. Geophys. Res., 95, 5983
McIntosh, S. W. 2009, ApJ, 693, 1306
McKean, M. E., Winglee, R. M., & Dulk, G. A. 1989, Sol. Phys., 122, 53
McKenzie, D. E., & Savage, S. L. 2009, ApJ, 697, 1569
Melrose, D. B. 1994, Space Sci. Rev., 68, 159
Melrose, D. B. 2009, in IAU Symp. 257, Universal Heliophysical Processes, ed. N. Gopalswamy & D. F. Webb (Cambridge: Cambridge Univ. Press), 305
Melrose, D. B., & Dulk, G. A. 1982, ApJ, 259, 844
Melrose, D. B., Hewitt, R. G., & Dulk, G. A. 1984, J. Geophys. Res., 89, 897
Messmer, P., & Benz, A. O. 2000, A&A, 354, 287
Mozer, F. S., & Kletzing, C. A. 1998, Geophys. Res. Lett., 25, 1629
Mutel, R. L., Christopher, I. W., & Pickett, J. S. 2008, Geophys. Res. Lett., 35, L07104
Neidig, D., Wiborg, P., Confer, M., et al. 1998, in ASP Conf. Ser. 140, Synoptic Solar Physics, ed. K. S. Balasubramaniam, J. Harvey, & D. Rabin (San Francisco, CA: ASP), 519
Persoon, A. M., Gurnett, D. A., & Shawhan, S. D. 1983, J. Geophys. Res., 88, 10123
Pritchett, P. L. 1984, J. Geophys. Res., 89, 8957
Pritchett, P. L., & Strangeway, R. J. 1985, J. Geophys. Res., 90, 9650
Pritchett, P. L., Strangeway, R. J., Carlson, C. W., et al. 1999, J. Geophys. Res., 104, 10317
Pritchett, P. L., Strangeway, R. J., Ergun, R. E., & Carlson, C. W. 2002, J. Geophys. Res., 107, 1437
Ramaty, R. 1979, in AIP Conf. Proc. 56, Particle Acceleration Mechanisms in Astrophysics, ed. J. Arons, C. McKee, & C. Max (Melville, NY: AIP), 135
Robinson, P. A. 1989, ApJ, 341, L99
Roux, A., Hilgers, A., de Feraudy, H., et al. 1993, J. Geophys. Res., 98, 11657
Slottje, C. 1978, Nature, 275, 520
Slottje, C. 1980, in IAU Symp. 86, Radio Physics of the Sun, ed. M. R. Kundu & T. E. Gergely (Dordrecht: Reidel), 195
Slottje, C. 1981, Atlas of Fine Structures of Dynamic Spectra of Solar Type IV-dm and Some Type II Radio Bursts (Utrecht: Publ. Utrecht Observatory), 90
Stasiewicz, K., Bellan, P., Chaston, C., et al. 2000, Space Sci. Rev., 92, 423
Strangeway, R. J., Kepko, L., Elphic, R. C., et al. 1998, Geophys. Res. Lett., 25, 2065
Švestka, Z. 2007, Sol. Phys., 246, 393
Tanaka, H., & Kakinuma, T. 1962, J. Phys. Soc. Japan, 17, 211
Temerin, M. 1984, J. Geophys. Res., 89, 3945
Temerin, M., Cerny, K., Lotko, W., & Mozer, F. S. 1982, Phys. Rev. Lett., 48, 1175
Treumann, R.A. 2006, A&AR, 13, 229
Tsuneta, S., Ichimoto, K., Katsukawa, Y., et al. 2008, Sol. Phys., 249, 167
White, S. M., Melrose, D. B., & Dulk, G. A. 1983, PASA, 5, 188
White, S. M., Melrose, D. B., & Dulk, G. A. 1986, ApJ, 308, 424
Winglee, R. M., & Pritchett, P. L. 1986, J. Geophys. Res., 91, 13531
Wu, C. S., & Lee, L. C. 1979, ApJ, 230, 621
Zheleznyakov, V. V., & Zaitsev, V. V. 1975, A&A, 39, 107